UNIVERSITY OF CALIFORNIA SAN DIEGO

Using In-vivo Two Photon Microscopy to Investigate the Dentate Gate Hypothesis

A Thesis submitted in partial satisfaction of the requirements for the degree Master of Science

in

Biology

by

Shannon Huey-Ruey Kee

Committee in Charge:

Professor Matthew Shtrahman, Chair
Professor Brenda Bloodgood, Co-Chair
Professor James Cooke

2021

The Thesis of Shannon Huey-Ruey Kee is approved, and it is acceptable in quality and form for publication on microfilm and electronically.

University of California San Diego

2021

TABLE OF CONTENTS

LIST OF FIGURES

ACKNOWLEDGEMENTS

I wish to express my deepest gratitude to my mentor and advisor, Dr. Matthew Shtrahman, for his unwavering support and guidance. I would also like to express my sincere thanks to Dr. Brenda Bloodgood and Dr. James Cooke for serving on my thesis committee and supporting my research efforts. I am also extremely grateful for the contributions and support of Stacy Kim, Adrian Martinez, Summer Batasin, Alexander Newberry, Weilun Yao, Emily Ferguson, Thanh Tran, Dr. Fred Gage, and Ondrej Novak.

ABSTRACT OF THE THESIS

Using In-vivo Two Photon Microscopy to Investigate the Dentate Gate Hypothesis

by

Shannon Huey-Ruey Kee

Master of Science in Biology

University of California San Diego, 2021

Professor Matthew Shtrahman, Chair
Professor Brenda Bloodgood, Co-Chair

The most common form of focal epilepsy in adults is mesial temporal lobe epilepsy (mTLE). Evidence points to the hippocampal formation as a key site of epileptogenesis of mTLE, but its mechanisms remain unknown. The dentate gate hypothesis has been a major mechanistic concept in epilepsy for over 20 years which posits that the sparse firing of the dentate gyrus acts as a ‘gate’ that prevents

overexcitation of hippocampal circuits that lead to epilepsy. Using in vivo two-photon microscopy and surgical implantation of a chronic cranial imaging window, we were able to study the network activity within the hippocampus in awake mice. Consistent with the dentate gate hypothesis, we found increased hyperexcitability in the dentate gyrus of epileptic mice using a status epilepticus (SE) model in which SE was induced at 6 weeks of age or older. Surprisingly, mice induced with SE at 3 weeks of age did not develop hyperexcitability. The results of this study will be used to further study the pathophysiological and electrophysiological differences between younger and older mice induced with SE.

Chapter 1. Introduction

Mesial Temporal Lobe Epilepsy

Mesial temporal lobe epilepsy (MTLE) is the most common form of acquired focal epilepsy in adults. In addition to recurrent disabling seizures and shortened life expectancy, patients suffer from accompanying cognitive and psychiatric impairments; gradual deterioration of memory, attention, mood, and executive functions are common. Pathologically, the most common change is atrophy and astrogliosis of the hippocampus leading to hippocampal sclerosis (Engel et al 2001).

Treatment options include antiepileptic medication, vagus nerve stimulation, and temporal lobectomy (Devinsky 2004). However, about 30- 40% of MTLE patients cannot control seizures with available treatments (Tatum 2012). Antiepileptic medications can greatly reduce seizure frequency but require significant risk-benefit consideration, with disabling side effects on the patient's social, emotional, and cognitive abilities. Vagus nerve stimulation serves as an adjuvant therapy aimed to modestly reduce medication dosage. The most medically effective treatment is temporal lobe surgery; over 70% of patients that undergo temporal lobectomies are freed of seizures. (Devinsky 2004). However, the highly invasive procedure presents numerous complications with verbal memory and language deficits being the most common. (Sherman et al. 2011). In addition, 15% of patients evaluated for surgery are not eligible (Helmstaedter et al. 2014).

The Hippocampal Formation

The hippocampal formation is located in the medial temporal lobe of the brain and can be defined as encompassing the dentate gyrus (DG), the hippocampus proper (CA1-4), the subiculum, and the entorhinal cortex (EC). The dentate gyrus can be roughly divided into three

layers: the molecular layer, the granule cell layer, and the hilus (polymorphic layer). The molecular layer is comprised of the dendrites that originate from the densely packed glutamatergic granule cells of the granule cell layer. The hilus contains the axons (mossy fibers) of the granule cells, GABAergic interneurons, and hilar mossy cells, among others (Amaral 2007, Scharfman 2016).

The hippocampal network is primarily uni-directional and is known as the tri-synaptic loop. Cortical sensory information being funneled through layer two of the EC is sent to the DG via the perforant path. DG neurons then synapse onto CA3 pyramidal neurons via the mossy fiber pathway. CA3 neurons then send information to CA1 pyramidal neurons through the Schaffer Collateral pathway. CA1 neurons synapse onto the subiculum, which then sends the output back into the EC, or can also synapse directly onto the EC to complete the loop. In addition to the trisynpatic loop, the DGCs can also directly connect to the CA1 pyramidal neurons via the temporammonic pathway. Information can also flow directly from the EC to CA3 neurons (Knierim 2015).

Sparse Firing of the Dentate Gyrus

A key characteristic of the DG is its sparse neural activity. In contrast to the directly upstream activity of the EC in which the percentage of active neurons and their mean firing rates is high, the encoding scheme of the DG is characterized by a very low proportion of active neurons whose mean firing rates are also low (Barnes et al. 1990, Piatti et al. 2013). It has been theorized that cortical input funneled through the small population of EC cells is distributed to a larger amount of DGCs, allowing the DGCs to augment small differences in input (Leutgeb 2007).

Several mechanisms have been theorized to be contributing to the sparse firing of DGCs. Intrinsically, DGCs have relatively hyperpolarized membrane potentials in comparison to other hippocampal neurons, at about -85mV, requiring larger inputs to generate an action potential (Staley et al. 1992). There is also a relatively stronger voltage attenuation of EPSPs in granule cell dendrites and a lack of dendritic spiking, which would also contribute the low spiking activity of DGCs (Krueppel 2011, Nevian 2007).

The surrounding inhibitory network interacting with DGCs also likely contributes to sparse firing. Feedforward hilar interneurons are more easily recruited by activation of the perforant path than DGCs, more likely leading to a greater summation of inhibitory potentials rather than excitatory potentials (Scharfman 1991, Ewell and Jones 2010). The primary postsynaptic targets of mossy fibers of DGCs are hilar interneurons, many of which are somatostatin positive (Acsady et al. 1998). This has been suggested to be evident that the DG is a competitive network in which activated DGCs excite interneurons that inhibit other DGCs (Rolls 2010). Together, the feedforward and feedback mechanisms of hilar interneurons are thought to be a significant factor in the DG's sparse network activity.

Adult Neurogenesis in the Dentate Gyrus

Adult born neurons are also thought to be a significant factor in regulating the DG's sparse network, and approximately 3% of DGCs are newborn neurons (Piatti et al. 2013, Cameron and Mckay 2001). The hippocampus is one of two areas of adult mammalian brain known to generate new neurons. Immature DGCs are born in the subgranular zone (SGZ) of the DG and take six to eight weeks to mature and integrate into the network, and their development can be categorized into five stages. Quiescent radial glial- like neural progenitor cells reside in the SGZ (type 1) and can give rise to intermediate proliferating cells (type 2) in approximately

three days. Type 2 cells can then give rise to neuroblasts (type 3) within a week after birth. In the next two weeks, these neuroblasts then differentiate into immature DGCs (Goncalves 2016) Finally, at 6-8 weeks after birth, the DGCs are functionally and structurally similar to that of fully mature DGCs, though it takes several more weeks until the adult-born DGCs are electrophysiologically indistinguishable from fully mature DGCs (van Praag et al. 2002).

Adult Neurogenesis and Sparse Firing of the DG

Evidence suggests that adult-born DGCs play a key role in regulating hippocampal activity. Particularly, newborn neurons at 4-6 weeks of age have distinct characteristics from their mature counterparts, including a high intrinsic excitability and unique local circuit interactions (Piatti et al. 2013).

It has been the prevailing idea that adult-born DGCs contribute to the excitability of the DG. DGCs more readily fire action potentials in response to weak excitatory inputs due to a high input resistance and low threshold T-Type calcium channels (Schmidt-Hieber et al. 2004; Mongiat et al. 2009). They also have a higher resistance to perisomatic GABAergic inhibition (Marin-Burgin et al. 2012). It has also been indicated that adult-born DGCs have enhanced synaptic plasticity during a critical period of 4-6 weeks old with increased LTP amplitude and decreased LTP induction threshold (Ge et al, 2007).

However, there has been accumulating evidence that adult-born DGCs could contribute to the sparse activity of the DG instead. Anatomically, both mature and immature DGCs directly innervate hilar interneurons, each inhibiting hundreds of mature DGCs (Freund and Buzsaki 1996). DGCs also innervate excitatory hilar mossy cells, which synapse onto local interneurons and DGCs on the contralateral DG (Scharfman, 1995). Their mossy fiber boutons are also small, suggesting that their primary targets are GABAergic interneurons (Acsady et al. 1998; Ide et al.

2008; Toni et al, 2008). It has also been shown that in-vivo elimination of newborn DGCs less than 6 weeks old in anesthetized mice resulted in an increase of gamma-frequency burst amplitude in the DG and hilus, along with an increase in synchrony of DG action potentials during gamma bursts (Lacefield et al. 2012). Therefore, it is possible that immature DGCs have an overall inhibitory effect in which their potent excitability recruits inhibitory neurons to help quiet the DG.

Pathophysiology of mTLE

The most common pathological change in mTLE is atrophy and astrogliosis of the hippocampus leading to hippocampal sclerosis (Engel et al 2001). Cellular abnormalities include mossy fiber sprouting, increased proliferation of neural progenitors, aberrant hippocampal neurogenesis, hilar ectopic dentate granule cells (DGCs), hypertrophy of hippocampal astrocytes and microglia, loss of inhibitory hilar interneurons (Parent and Kron 2012, Cho et al. 2015, Hosford et al. 2016, Houser 2014).

Mossy fiber sprouting refers to the development of abnormal mossy fiber synapses. Normally, the axons of DGCs project along the mossy fiber pathway to CA3 and hilus, with rare recurrent synapses onto DGCs (Parent and Kron 2012). However, in epileptic animals, Timm staining demonstrated aberrant sprouting in the dentate inner molecular layer and electron microscopy indicated the creation of recurrent excitatory through synapses onto neighboring DGCs (Mello et al. 1993; Okazaki et al. 1995). Additionally, it has been shown that only DGCs at 2-4 weeks old at the time of status epilepticus (SE) contribute to mossy fiber sprouting (Jessberger 2007).

It has also been suggested that newborn DGCs are both necessary and sufficient for the formation of seizures in epilepsy. Inducible and reversible chemogenetic (DREADD) mediated

specific suppression of newborn DGCs lead to a decrease in seizures and specific activation lead to an increase in seizure activity. Retrograde tracing revealed that newborn DGCs during epilepsy demonstrate formation of excessive excitatory networks with increased inputs from the EC, recurrent excitatory loops within the DG, and reciprocal connections between DGCs and CA3 pyramidal neurons (Zhou et al. 2019).

Hilar ectopic granule cells are also a common finding in epileptic animals and may be contributing to the development of recurrent seizures. Instead of migrating to the granule cell layer, granule cells born in the SGZ migrate into the hilus or to the molecular layer (Parent et al. 1997). In addition, only DGCs born after SE migrate aberrantly (Kron et al. 2010).

Two-Photon Microscopy

Two-photon microscopy is an imaging technique that allows for extended imaging in live tissue several hundred microns deep at single cell resolution. The technique utilizes two low energy photons to simultaneously excite a fluorophore that causes the subsequent emission of a higher energy photon. Two-photon excitation occurrence depends quadratically with excitation intensity, therefore, more fluorescence generated in the area of focus. As a result, in contrast to one photon microscopy, two-photon microscopy reduces phototoxicity and photobleaching to only the plane of focus while increasing the single-to-noise ratio. The use of low energy, long wavelength photons, typically around the infrared range, also minimizes light scattering and therefore signal loss (Denk et al. 1994).

Red Shifted Genetically Coded Ca^{2+} Indicators

In this study we utilized mApple based jRGECO1a, a new generation red shifted calcium indicator for monitoring neural activity (Dana et al. 2016). Genetically encoded calcium indicators allow for noninvasive measurement of neuronal populations in-vivo. Red

fluorophores, particularly those in the near infrared region (~650-1000nm), have advantages of increased tissue penetration due to minimal absorption by water and hemoglobin, as well as lower phototoxicity and lower autofluorescence due to lower wavelength excitation (Schenkman et al. 1999, Wu et al. 2013). Red shifted genetically coded calcium indicators are based on circularly permutated red fluorescent proteins (RFPs) in which its N terminus is fused to the calmodulin binding region of chicken myosin light chain kinase (M13), and its C terminus is fused calmodulin (CaM). Binding of Ca^{2+} results in the association of CaM and M13, causing a change in the environment and an increase in fluorescence (Zhao et al. 2011). Calcium indicators can be used to indirectly measure neural activity because presynaptic depolarization with action potentials causes voltage gated calcium channels to open and result in an influx of calcium. The resulting calcium transients allow for neural activity to be visualized through optical methods. (Chen et al., 2013).

Pilocarpine Murine Model of Temporal Lobe Epilepsy

In this study we utilized the pilocarpine murine model of temporal lobe epilepsy, a widely used chronic animal model that reproduces the etiology and pathophysiology of human medial temporal lobe epilepsy (Curia et al., 2008). The human disease is characterized by an initial precipitating injury within the first 4-5 years of life, followed by a latent seizure free period, and finally the development of recurring afebrile spontaneous seizures with hippocampal sclerosis and network reorganization (Engel 2001). Similar to the human disease, the pilocarpine model includes an initial precipitating injury in the form of pilocarpine induced status epileptics (SE), followed by a latent seizure free period, and finally onset of spontaneous recurrent seizures with similar limbic lesions and network reorganization (Curia et al. 2008). Pilocarpine is a muscarinic agonist acting primarily through the M1 receptor causing an imbalance between excitatory and

inhibitory transmission to cause SE (Hamilton et al. 1997, Priel and Albuquerque 2002). SE is then thought to be maintained by NMDA receptor activation (Smolders et. al 1997).

Chapter 2. Materials and Methods

Animal Use.

All animal use and procedures followed protocols approved by the Institutional Animal Care and Use Committees of the University of California San Diego. All experiments were conducted in accordance with local, state, and federal guidelines for animal research. Three and six week old male mice at time of status epilepticus induction were used in this study. C57BL/6 mice were purchased from Charles Rivers Laboratories. Mice were housed in standard housing conditions, with up to four mice per cage, on a 12 hour light/dark cycle with food and water provided *ad libitum*.

Status epilepticus induction by pilocarpine.

To reduce peripheral cholinergic stimulation, mice at either three or six weeks old of age were treated with an intraperitoneal injection (i.p.) injection of 1mg/kg of N-methylscopolamine bromide (Sigma-Aldrich) 30 min prior to injection of pilocarpine hydrochloride (Sigma-Aldrich) (Clifford et al. 1987). Control mice received identical injections with the exception of saline substituting for pilocarpine. Mice then received an i.p. injection of a single dose of pilocarpine dependent on weight: 250mg/kg for mice weighing greater than 25kg, 275mg/kg for mice between 20 and 25kg, and 285mg/kg for mice less than 20kg. Mice were monitored for behavioral seizures. Additional subsequent doses of pilocarpine were administered thirty-five minutes after the initial dose if the mouse did not exhibit a behavioral seizure, and thirty-five

minutes after the mouse's last seizure if it did not enter SE. SE was defined as when a mouse had two or more Rancine Grade 3 seizures (forelimb clonus, rearing, and/or falling) followed by continuous Rancine Grade 2 seizing (head nodding) (Shibley and Smith 2002). After two hours in SE, seizures were terminated with diazepam (10mg/kg), and if seizure activity persisted, it was re-administered after 30 to 40 minutes. Soft food and an i.p. injection of 1ml of normal saline were administered the day after to aid in recovery.

Retrograde adeno-associated virus labeling of dentate granule cells.

DGCs were labeled with an attenuated retrograde recombinant adeno-associated virus (rAAV-retro) that expressed the red calcium indicator jRGECO1a under the control of the calcium/calmodulin-dependent kinase-α promoter CaMKIIα. Mice were deeply anesthetized with 5% isoflurane and maintained at 2% isoflurane and 0.5L/min in O_2 via a nose cone and placed in a stereotactic on a 37° C heating pad to maintain the mouse's body temperature. Prior to the surgery, mice received 2.5mg/kg i.p. dexamethazone to prevent swelling. The site was cleaned with 10% povidone-iodine and 70% ethanol prior to exposure of the dorsal skull. An injection hole in the skull was made using a standard pneumatic dental drill. Two injections of 400uL of rAAV8, in 23 nL pulses at 10 second intervals, were stereotactically administered in the right hemisphere using a microinjector (Nanoject III Auto-Nanoliter Injector) and a pulled glass capillary tube. The injection site at CA3 was determined by using the coordinates of bregma as reference: anterior/posterior, -1.8mm; lateral-1.8mm; dorsal/ventral movement of -1.6 and -1.9 mm. The injection capillary was kept at each injection site for a period of 7 minutes after the injection to allow the virus to diffuse. After removal of the injection capillary, the incision was closed using a cyanoacrylate adhesive. Mice recovered on a heating pad and

returned to their home cage to rest after regaining consciousness. Implantation surgery was performed two hours after viral injection.

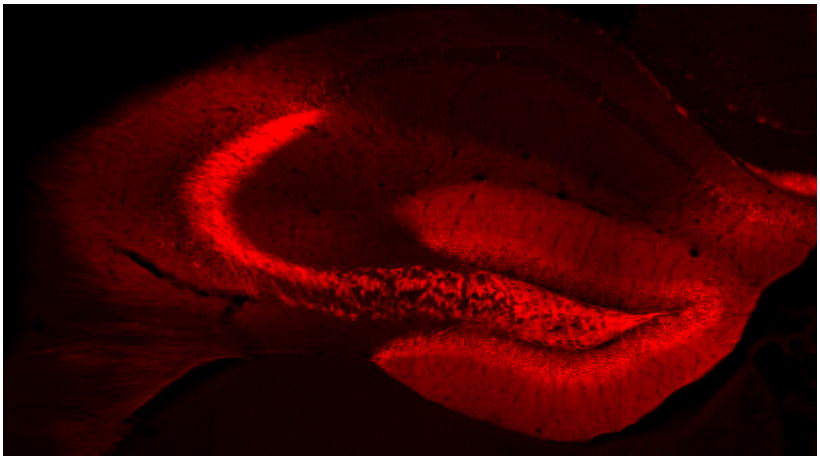

Figure 1. rAAV Labeling of DGCs. Injection at CA3 allows retrograde recombinant adeno-associated virus labeling of dentate granule neurons with red-shifted Ca2+ indicator jRGECO1a (rAAV-retro.CAMKII.jRGECO1a).

Aspiration and cranial window implantation surgery.

The craniotomy site was cleaned with applications of 70% ethanol and 10% provodine alternating each three times. The scalp was then removed to reveal the dorsal skull and connective tissue around the site was removed. OptiBond All-in-one dental adhesive was applied over the exposed skull and cured with UV light, to allow for better adhesion of the skull to dental resin. A 3mm diameter craniotomy around the virus injection site centered on the right hemisphere was performed using a standard pneumatic dental drill. The underlying dura mater was removed and the cortex and corpus callosum was aspirated using a blunt tip needle and a vacuum line. Sterile saline was used to irrigate the lesion, and gelfoam was used as a hemostatic. A 1.7mm deep titanium window implant with a 3mm #1 glass coverslip bottom was placed in the lesion. The window was secured using a layer of fast curing orthodontic acrylic resin applied

over the exposed scalp. A titanium bar was also attached using the orthodontic resin to the skull to allow for the animal to be secured to the microscope stage later on. Everything was secured with one final layer of orthodontic acrylic resin and allowed to dry. The mice were administered i.p. carprofen (5mg/kg) for inflammation and s.q. buprenorphine slow release (0.1mg/kg) for pain relief. The mice were then returned to their cages to recover. We have previously found that surgical implant and imaging procedures do not affect adult neurogenesis (see Goncalves 2016 Fig. S2.8 & S9).

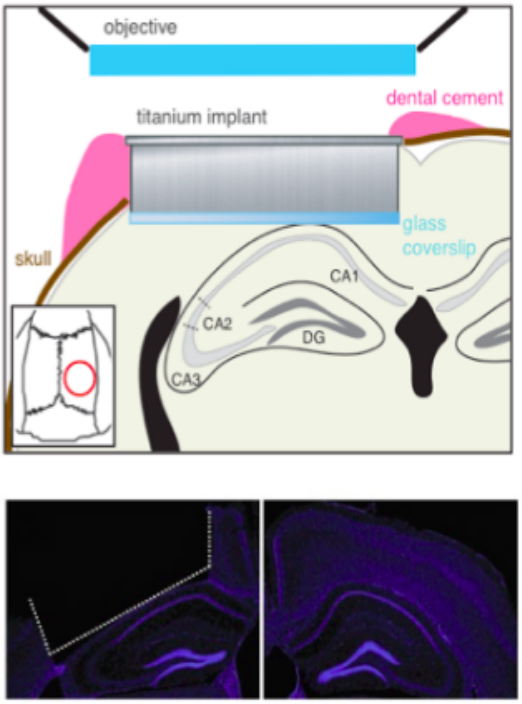

Figure 2. Aspiration and Cranial Window Implantation. Top: Schematic of chronic imaging window implanted above CA1, adapted from Goncalves et al Nat Neuroscience 2016. Bottom: DAPI-stained coronal section of mouse brain with implant (left) and control contralateral hemisphere (right).

Two-photon imaging of DGCs.

Mice placed on a treadmill and secured to a goniometer-mounted head-fixation apparatus. The plane of the cranial window coverslip was leveled perpendicular to the imaging path of the microscope objective using a custom-built laser alignment tool. Imaging was performed using a two photon laser scanning microscopy (MOM, Sutter Instruments) using a femtosecond-pulsed laser (Chameleon Ultra II, Coherent) fixed at 1050nm and a 16x water immersion objective (0.8NA, Nikon). ScanImage software written in MATLAB (Pologruto et al., 2003) was used to acquire 512x128 pixel videos at a frame rate of 3.91Hz. Images were obtained on multiple non consecutive days between eight and fifteen days post injection.

Tissue collection

A lethal dose of ketamine-xylazine (130mg/kg, 15mg/kg; i.p.) was used to deeply anesthetize mice before transcardial perfusions with 0.9% phosphate buffered sodium chloride followed by 4% paraformaldehyde in 0.1M phosphate buffer (pH 7.4). Brains were dissected, postfixed in 4% PFA for 24 hours and transferred to a 30% sucrose solution for at least 48 hours to equilibrate.

Statistical analysis

Two photon calcium imaging videos were analyzed using custom software developed by Alexander Newberry at the Gage Lab and Dr. Ondre Novak of Palacky University Olomouc. As mice were not trained or incentivized to run on the treadmill, they were stationary for most of recording time. First, image stabilization was performed using an algorithm that maximizes the correlation coefficient between each frame with a reference frame constructed from the average of the most stable frames of the video, and further improved upon with line-by-line alignment. Portions of the video below a defined cross-correlation stabilization threshold were discarded

(Fig 3a). The program then performs automatic cell segmentation by first scanning a ring shape with variable size and shape metrics across a motion corrected reference image, and then draws a region of interest when the cross-correlation metric crosses a user-defined threshold. The user may then remove false positives or label cells that were not automatically identified (Fig 3b). The program assigns each cell a number label and records signal intensity. To eliminate photo-bleaching effects, baseline fluorescence (F) was fit to an exponential curve. Finally, the program calculates the change in fluorescence over the baseline fluorescence per region of interest (%ΔF/F) over time. Single cell traces of fluorescence fluctuations are printed, and calcium related spiking activity was recorded, taking into account the fluorescence fluctuation amplitude and shape (Fig 3c). Active cells were defined as having at least one event in which fluorescence fluctuation (%ΔF/F) has amplitude > 7 standard deviations of the negative fluctuations of the %ΔF/F trace.

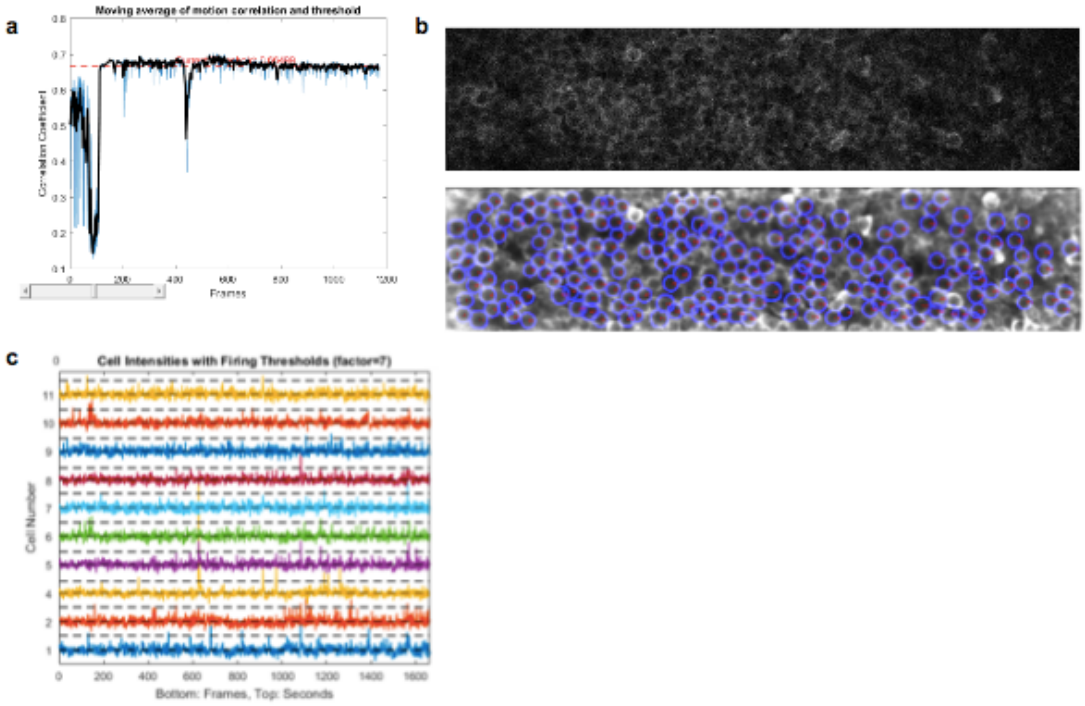

Figure 3. Analysis and Quantification of Calcium Activity (a) Plot of correlation coefficients assigned to each frame and selection of a stabilization threshold prior to motion correction (b) Cell segmentation with cells identified highlighted in blue and numbered in red (c) Single cell tracings of calcium fluorescence with firing thresholds indicated to identify fluorescence fluctuations (% ΔF/F) with amplitude > 7 SD above background noise.

Chapter 3. Results

Using the murine pilocarpine model of mesial temporal lobe epilepsy, with pilocarpine administered to induce status epilepticus and saline administered to control littermates, the spontaneous network activity of three cohorts of mice at varying ages were studied. All mice received unilateral stereotaxic injections of retro adeno-associated virus (rAAV-retro.CAMKII.jRGECO1a) to label excitatory neurons, followed by cranial window implantation one week before the start of two-photon in-vivo imaging. Mice were returned to the home cage within the animal vivarium in between surgery and imaging, and between imaging sessions. Images were taken on nonconsecutive days to minimize heat and power exposure on the brain. 2350 frame videos at 3.91fps were recorded and analyzed using custom MATLAB software.

The first cohort studied were mice that were induced with SE at 6-7 weeks old, received retro adeno-associated virus labeling and cranial window implantation at age of 14 or older, and were imaged at the age of 16 weeks or older (Fig 4). The level of spontaneous network activity in epileptic mice of this group indicated hyperexcitability in terms of percent active cells per minute (Fig 5), with the number of events per minute showing a similar but not statistically significant trend for events per minute (Fig 6). An active cell is defined as having at least one event. One event is defined as fluorescence fluctuation [$\Delta F/F$] with amplitude > 7 SD above background noise. However, yield was low due to due to poor imaging quality.

We hypothesized that younger mice would have a greater yield, and so we experimented with a second cohort in which the wait time between SE induction and viral injection was shortened. This next cohort were induced at 6-7 weeks old, received retro adeno-associated virus labeling and cranial window implantation at age of 10-11 weeks of age, and imaged at 12-13 weeks of age (Fig 4). The epileptic mice of this group indicated hyperexcitability of the DG in

which there are more active cells per minute (Fig 5) and a similar but non statistically significant trend for events per minute (Fig 6).

Additionally, we further experimented with a third younger cohort of mice in an effort to optimize imaging yield by inducing SE at a younger age with the same wait period between SE and viral injection as the previous cohort. This cohort was induced with SE at 3-4 weeks, administered retro adeno-associated virus labeling and cranial window implantation at 7-8 weeks of age, and imaged at 9-10 weeks of age (Fig 4). Surprisingly there was no significant difference in the network activity of these mice (Fig 5, Fig 6).

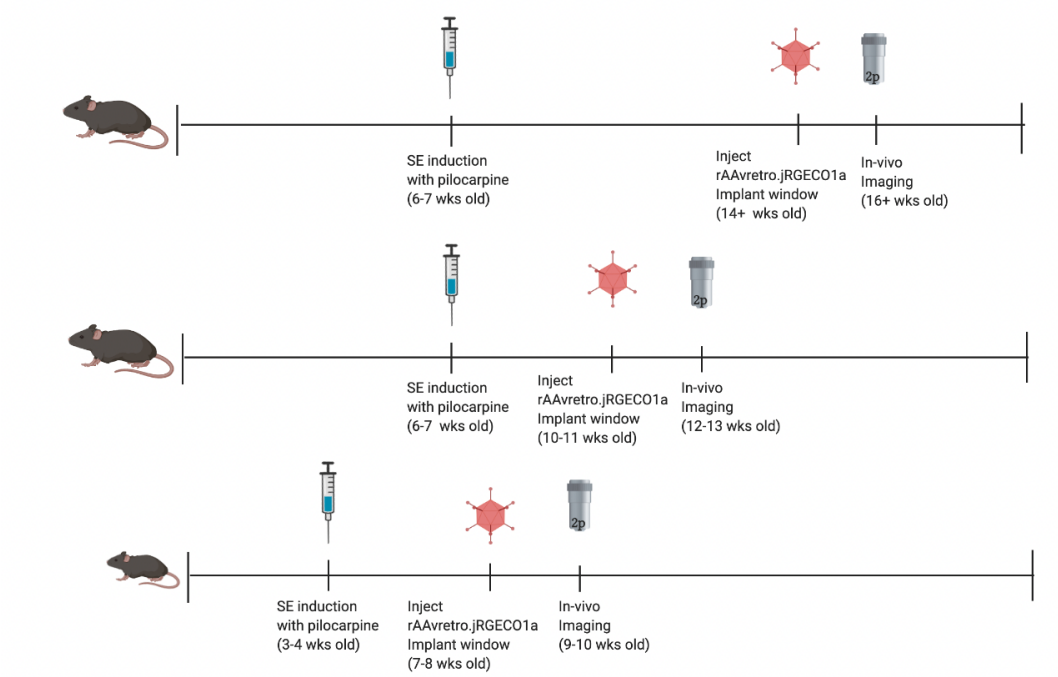

Figure 4. Timelines of Cohorts of Mice with Different Ages at Imaging. 3+ weeks after status epilepticus induction (SE), excitatory DGCs were labeled with rAAV.jRGECO1a and the cells were imaged at different time points from 9dpi-15dpi

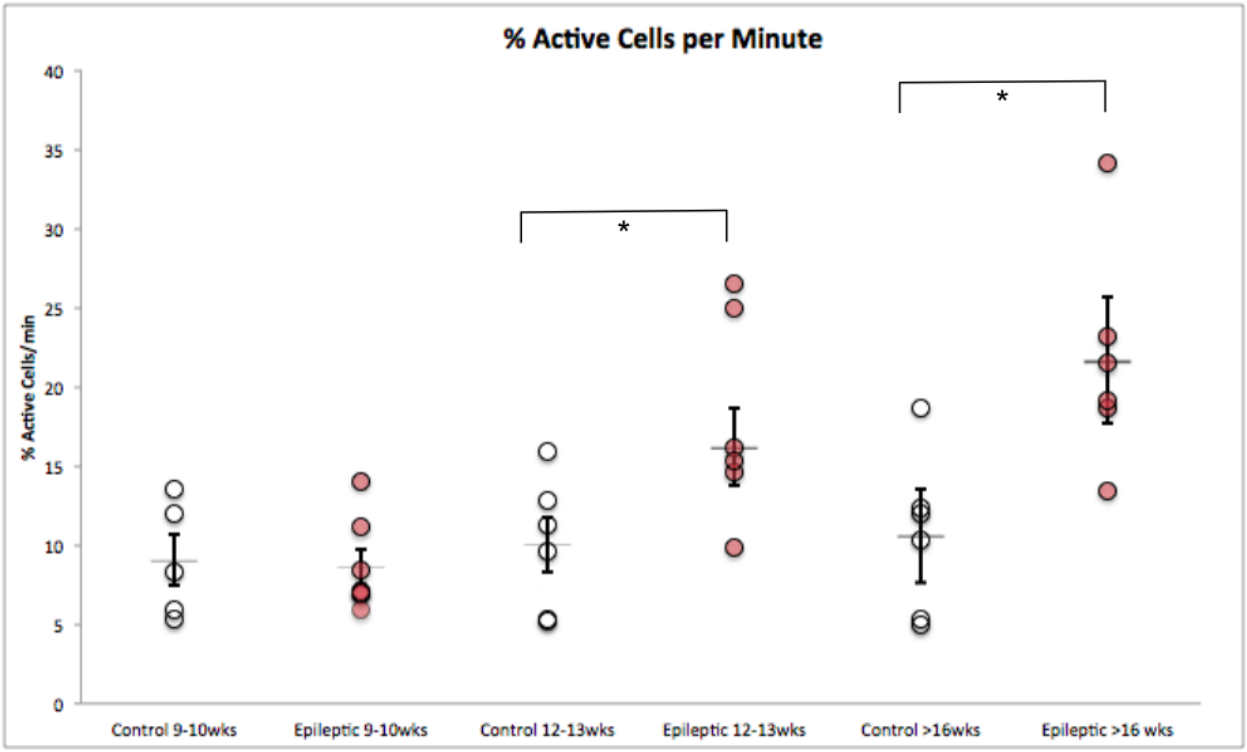

Figure 5. Level of Spontaneous Network Activity in Epileptic Mice: Amount of Active Cells. Mean (±SEM) percentage of active cells per field of view (% active cells) of control and epileptic cohorts of varying ages at imaging. Active cells are defined as having at least one response (fluorescence fluctuations [ΔF/F] with amplitude > 7 SD above background noise). Each dot represents one animal. Mann–Whitney U test (*) $p<0.05$

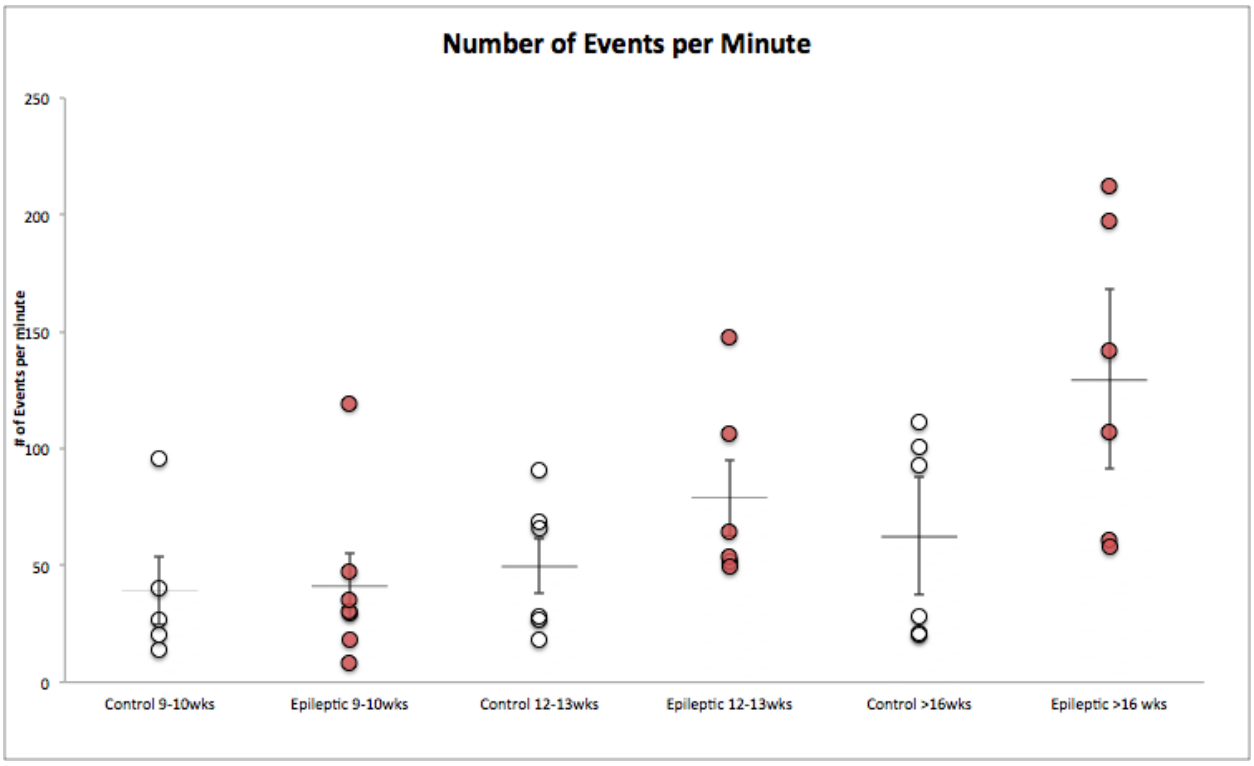

Figure 6. Level of Spontaneous Network Activity in Epileptic Mice: Activity of Active Cells. Mean (±SEM) number of events per min of control and epileptic cohorts of varying ages at imaging. Active cells are defined as having at least one event. One event is defined as a fluorescence fluctuation [ΔF/F] with amplitude > 7 SD above background noise). Each dot represents one animal. Mann–Whitney U test (*) $p<0.05$

Chapter 4. Discussion

In the study, we have obtained in-vivo data from awake behaving epileptic mice that is consistent with the dentate gate hypothesis in which the dentate gyrus loses its ability to 'gate' activity and becomes hyperexcitable in mTLE in mice that were induced with SE at 6 weeks of age or older. This was found through recording and quantifying the amount of spontaneous network activity of the DGCs in the dentate gyrus of epileptic mice. We also plan to develop a statical measure of synchrony to quantify synchrony in epileptic mice and determine if there is also increased synchrony in comparison to control mice.

Due to the low yield nature of this imaging method, we experimented with three different cohorts of mice of different ages at imaging to optimize yield and maximize sample size. We found old age correlated with poorer imaging quality. Possible factors contributing to poorer imaging results in older mice could be due to a larger brain size, increased myelination, or increased inflammation due to seizures in the epileptic cohorts.

Furthermore, the data shows that mice induced with SE at 6 weeks of age were found to be hyperexcitable, but not mice induced with SE at 3 weeks of age. This could indicate that younger mice may have a protective mechanism in place that protects them from epileptogenesis. We plan to further investigate the differences in electrophysiology between younger mice and older mice induced with SE with EGG. If the same finding is observed, we would like to propose using young mice induced with SE as a control that will enable further studies into determine what associated pathological features may be causative versus as a result of epileptogenesis.

The data also indicates a large variability within each cohort, and this was expected as the pilocarpine model is inherently variable (Curia et al. 2008). To further investigate this variability, we plan to look for possible correlations between the level of activity and histological analysis of

key pathological features of mTLE: mossy fiber sprouting, increased proliferation of neural stem cells and aberrant neurogenesis, increased ectopic dentate granule cells, increased inflammation, increased loss of mossy cells, and loss of inhibitory neurons. We hope this will also help pinpoint which pathological features are strongly correlated with increased hyperactivity.

References

Acsady L., Kamondi A., Sík A., Freund T., Buzsáki G. (1998). GABAergic cells are the major postsynaptic targets of mossy fibers in the rat hippocampus J. Neurosci., 18 , pp. 3386-3403

Amaral D. G., Scharfman H. E., & Lavenex, P. (2007). The dentate gyrus: fundamental neuroanatomical organization (dentate gyrus for dummies). Progress in brain research, 163, 3–22. doi:10.1016/S0079-6123(07)63001-5

Barnes C. A., McNaughton B. L., Mizumori S. J., Leonard B. W., and Lin L. H. (1990). Comparison of spatial and temporal characteristics of neuronal activity in sequential stages of hippocampal processing. Prog. Brain Res. 83, 287–300.

Cameron H. A., McKay R. D. (2001). Adult neurogenesis produces a large pool of new granule cells in the dentate gyrus. J. Comp. Neurol. 435, 406–417

Chen T. W., Wardill T., Sun Y., Pulver S. R., Renninger S. L., Baohan A., Schreiter E. R., Kerr R. A., Orger M. B., Jayaraman V., Looger L. L., Svoboda K., Kim D. S. Ultrasensitive fluorescent proteins for imaging neuronal activity. Nature 499**,** 295–300 (2013). doi: 10.1038/nature12354

Cho K. O., Lybrand Z. R., Ito N., Brulet R., Tafacory F., Zhang L., Good L., Ure K., Kernie S.G., Birnbaum SG, Scharfman HE, Eisch AJ, Hsieh J. (2015) Nat Commun., 6():6606.

Clifford D. B., Olney J. W., Maniotis A., Collins R. C., Zorumski C. F. (1987) The functional anatomy and pathology of lithium-pilocarpine and high-dose pilocarpine seizures. Neuroscience, 23:953–968.

Dana H., Sun Y., Hasseman J. P., Tsegaye G., Holt G. T., Fosque B. F., Schreiter E. R., Brenowitz S. D., Jayaraman V., Looge L. L., Svoboda K., Kim, D. S. (2016) Sensitive red protein calcium indicators for imaging neural activity. eLife 5, e12727

Denk W., Delaney K. R., Gelperin A., Kleinfeld D., Strowbridge B. W., Tank D. W., Yuste R., (1994) Anatomical and functional imaging of neurons using 2-photon laser scan-ning microscopy. J. Neurosci. Methods 54, 151–162

Devinsky O. (2004) Diagnosis and treatment of temporal lobe epilepsy. Rev Neurol Dis, 1(1):2-9.

Engel J., Jr. (2001) Mesial temporal lobe epilepsy: what have we learned? Neuroscientist. ;7:340–352. doi: 10.1177/107385840100700410.

Ewell L. A., Jones M. V. (2010). Frequency-tuned distribution of inhibition in the dentate gyrus. J. Neurosci. 30, 12597–12607 10.1523/JNEUROSCI.1854-10.2010

Freund T. F., Buzsaki G. (1996) Interneurons of the hippocampus. Hippocampus. 6:347–470.

Ge S., Yang C. H., Hsu K. S., Ming G. L., Song H. (2007). A critical period for enhanced synaptic plasticity in newly generated neurons of the adult brain. Neuron 54, 559–566 10.1016/j.neuron.2007.05.002

Gonçalves J. T., Schafer S. T., Gage F. H. (2016) Adult neurogenesis in the hippocampus: from stem cells to behavior. Cell, 167(4):897–914. doi: 10.1016/j.cell.2016.10.021.

Greenberg D. S., Houweling A. R., Kerr J. N. Population imaging of ongoing neuronal activity in the visual cortex of awake rats. Nat Neurosci. 2008 Jul;11(7):749-51. doi: 10.1038/nn.2140. Epub 2008 Jun 15.

Hamilton S. E., Loose M. D., Qi M., Levey A. I., Hille B., McKnight G. S. (1997) Disruption of the m1 receptor gene ablates muscarinic receptor-dependent M current regulation and seizure activity in mice. Proc Natl Acad Sci USA. 94:13311–13316.

Helmstaedter, C., Tw, M., von Lehe, M., M, v. L., Pfaefflin, M., Ebner, A., Pannek, H. W., Elger, C. E., Stefan, H. & Schramm, J. (2014) Temporal lobe surgery in Germany from 1988 to 2008: diverse trends in etiological subgroups. European Journal of Neurology 6, 827-834 .

Hosford B. E., Liska J. P., Danzer S. C., (2016) Ablation of Newly Generated Hippocampal Granule Cells Has Disease-Modifying Effects in Epilepsy. J Neurosci 36, 11013–11023. doi: 10.1523/jneurosci.1371-16.2016

Houser C. R., Do Structural Changes in GABA Neurons Give Rise to the Epileptic State? Advances in Experimental Medicine and Biology 813, 151-160 (2014).

Ide Y., Fujiyama F., Okamoto-Furuta K., Tamamaki N., Kaneko T., Hisatsune T. (2008). Rapid integration of young newborn dentate gyrus granule cells in the adult hippocampal circuitry. Eur. J. Neurosci. 28, 2381–2392 10.1111/j.1460-9568.2008.06548.x

Jessberger S., Zhao C., Toni N., Clemenson G. D Jr., Li Y,. Gage F. H. (2007).Seizure-associated, aberrant neurogenesis in adult rats characterized with retrovirus-mediated cell labeling. J Neurosci., 27(35):9400–9407.

Knierim, J. J. (2015). The hippocampus. Curr. Biol. 25, R1116–R1121.

Kron M.M., Zhang H., Parent J.M. (2010) The developmental stage of dentate granule cells dictates their contribution to seizure-induced plasticity.J Neurosci., 30(6):2051–2059.

Krueppel R., Remy S., Beck H., (2011). Dendritic integration in hippocampal dentate granule cells Neuron, 71, pp. 512-528

Lacefield C. O., Itskov V., Reardon T., Hen R., Gordon J. A. (2012). Effects of adult-generated granule cells on coordinated network activity in the dentate gyrus. Hippocampus 22, 106–116 10.1002/hipo.20860

Leutgeb J. K., Leutgeb S., Moser M. B., & Moser E. I. (2007). Pattern separation in the dentate gyrus and CA3 of the hippocampus. Science 315, 961–966

Marin-Burgin A., Mongiat L. A., Pardi M. B., Schinder A. F. (2012) Unique Processing During a Period of High Excitation/Inhibition Balance in Adult-Born Neurons. Science (Epub ahead of print)

Mello L. E., Cavalheiro E. A., Tan A. M., Kupfer W. R., Pretorius J. K., Babb T. L., Finch D. M. (1993) Circuit mechanisms of seizures in the pilocarpine model of chronic epilepsy: cell loss and mossy fiber sprouting. Epilepsia. 11–12;34(6):985–995.

Mongiat L. A., Esposito M. S., Lombardi G., Schinder A. F. (2009). Reliable activation of immature neurons in the adult hippocampus. PLoS ONE 4:e5320 10.1371/journal.pone.0005320

Nevian, T., Larkum, M. E., Polsky, A., and Schiller, J. (2007). Properties of basal dendrites of layer 5 pyramidal neurons: a direct patch-clamp recording study. Nat. Neurosci. 10, 206–214.

Okazaki M. M., Evenson D. A., Nadler J. V. (1995) Hippocampal mossy fiber sprouting and synapse formation after status epilepticus in rats: Visualization after retrograde transport of biocytin. J Comp Neurol., 352(4):515–534.

Parent J. M, Kron M. M. Neurogenesis and Epilepsy. In: Noebels J. L, Avoli M., Rogawski M.A., et al., editors. (2012) Jasper's Basic Mechanisms of the Epilepsies [Internet]. 4th edition. Bethesda (MD): National Center for Biotechnology Information (US).

Parent J. M., Yu T. W., Leibowitz R. T., Geschwind D. H., Sloviter R. S., Lowenstein D. H. (1997). Dentate granule cell neurogenesis is increased by seizures and contributes to aberrant network reorganization in the adult rat hippocampus. J Neurosci. May 15;17(10):3727–3738.

Piatti, V. C., Ewell, L. A. & Leutgeb, J. K. (2013). Neurogenesis in the dentate gyrus: carrying the message or dictating the tone. Frontiers in Neuroscience 7, doi:10.3389/fnins.2013.00050.

Pologruto T. A, Sabatini B. L, Svoboda K. (2003) ScanImage: Flexible software for operating laser scanning microscopes. Biomed. Eng. 2:13.

Priel M. R., Albuquerque E. X. (2002) Short-term effect of pilocarpine on rat hippocampal neurons in culture. Epilepsia. 43(Suppl 5):40–46.

Rolls E. T. (2010). A computational theory of episodic memory formation in the hippocampus. Behav. Brain Res. 215, 180–196 10.1016/j.bbr.2010.03.027

Scharfman H. E. (1991). Dentate hilar cells with dendrites in the molecular layer have lower thresholds for synaptic activation by perforant path than granule cells. J. Neurosci. 11, 1660–1673

Scharfman H. E. (1995). Electrophysiological evidence that dentate hilar mossy cells are excitatory and innervate both granule cells and interneurons. J. Neurophysiol. 74, 179–194

Scharfman H. E. (2016). The enigmatic mossy cell of the dentate gyrus. Nature reviews. Neuroscience, 17(9), 562–575. doi:10.1038/nrn.2016.87

Schenkman K. A., Marble D. R., Feigl E. O., Burns D. H. (1999) Near-infrared spectroscopic measurement of myoglobin oxygen saturation in the presence of hemoglobin using partial least-squares analysis. Appl Spectrosc ;53:325–331.

Schmidt-Hieber C., Jonas P., Bischofberger J. (2004). Enhanced synaptic plasticity in newly generated granule cells of the adult hippocampus. Nature.,429:184–187.

Sherman E. M., Wiebe S., Fay-McClymont T. B., Tellez-Zenteno J., Metcalfe A., Hernandez-Ronquillo L., Hader W. J., Jette N. (2011). Neuropsychological outcomes after epilepsy surgery: systematic review and pooled estimates. Epilepsia

Shibley H., Smith B. N. Pilocarpine-induced status epilepticus results in mossy fiber sprouting and spontaneous seizures in C57BL/6 and CD-1 mice. (2002) Epilepsy Res. 2002;49:109–120. doi: 10.1016/S0920-1211(02)00012-8.

Smolders I., Khan G. M., Manil J., Ebinger G., Michotte Y. (1997) NMDA receptor-mediated pilocarpine-induced seizures: characterization in freely moving rats by microdialysis. Br J Pharmacol. 121:1171–1179.

Staley K. J., Otis T. S., Mody I. (1992). Membrane properties of dentate gyrus granule cells: comparison of sharp microelectrode and whole-cell recordings. J Neurophysiol. May;67(5):1346-58.

Tatum W. O. (2012) Mesial temporal lobe epilepsy. Journal of Clinical Neurophysiology

Toni N., Laplagne D. A., Zhao C., Lombardi G., Ribak C. E., Gage F. H.,Schinder A.F,. (2008). Neurons born in the adult dentate gyrus form functional synapses with target cells. Nat. Neurosci. 11, 901–907 10.1038/nn.2156

van Praag H., Schinder A. F., Christie B. R., Toni N., Palmer T. D., Gage F. H. (2002) Functional neurogenesis in the adult hippocampus. Nature.415(6875):1030–1034. doi: 10.1038/4151030a.

Wu J., Liu L., Matsuda T., Zhao Y., Rebane A., Drobizhev M., Chang Y. F., Araki S., Arai Y., March K., Hughes T. E., Sagou K., Miyata T., Nagai T., Li W., Campbell R .E. (2013) Improved orange and red Ca(2)+/− indicators and photophysical considerations for optogenetic applications. ACS Chem. Neurosci. ;4:963–972. doi: 10.1021/cn400012b.

Zhao Y., Araki S., Wu J., Teramoto T., Chang Y. F., Nakano M., Abdelfattah S. A., Manabi F., Ishihara T., Nagai T., Takeharu N., Campbell R. E. (2011) An Expanded Palette of Genetically Encoded Ca2+ Indicators. Science.;333: 1888–1891. 10.1126/science.1208592

Zhou Q. G., Nemes A. D., Lee D., Ro E. J., Zhang J., Nowacki A. S., Dymecki S. M., Najm I. M., Suh H. (2019) Chemogenetic silencing of hippocampal neurons suppresses epileptic neural circuits. J Clin Invest 129:310–323.